

*Inorg Chem.* Author manuscript; available in PMC 2013 February 01

Published in final edited form as:

Inorg Chem. 2011 October 17; 50(20): 10460–10471. doi:10.1021/ic2016462.

# Di-peptide Based Models of Nickel Superoxide Dismutase: Solvent Effects Highlight a Critical Role to Ni-S Bonding and Active Site Stabilization

Eric M. Gale, Darin M. Cowart, Robert A. Scott, and Todd C. Harrop
Department of Chemistry, University of Georgia, 1001 Cedar Street, Athens, Georgia 30602

Todd C. Harrop: tharrop@chem.uga.edu

## **Abstract**

Nickel superoxide dismutase (Ni-SOD) catalyzes the disproportionation of the superoxide radical to O<sub>2</sub> and H<sub>2</sub>O<sub>2</sub> utilizing the Ni(III/II) redox couple. The Ni center in Ni-SOD resides in an unusual coordination environment that is distinct from other SODs. In the reduced state (Ni-SOD<sub>red</sub>), the Ni(II) center is ligated to a primary amine-N from His1, anionic carboxamido-N/ thiolato-S from Cys2, and a second thiolato-S from Cys6 to complete a NiN2S2 square-planar coordination motif. Utilizing the dipeptide N<sub>2</sub>S<sup>2-</sup> ligand, H<sub>2</sub>N-Gly-L-Cys-OMe (GC-OMeH<sub>2</sub>) that accurately models the structural and electronic contributions provided by His1 and Cys2 in Ni-SOD<sub>red</sub>, we have constructed the dinuclear sulfur-bridged metallosynthon, [Ni<sub>2</sub>(GC-OMe)<sub>2</sub>] (1). From 1 we have prepared the following monomeric Ni(II)-N<sub>2</sub>S<sub>2</sub> complexes: K[Ni(GC-OMe)  $(SC_6H_4-p-C1)$ ] (2),  $K[Ni(GC-OMe)(S^tBu)]$  (3),  $K[Ni(GC-OMe)(SC_6H_4-p-OMe)]$  (4), and K[Ni(GC-OMe)(S-NAc)] (5). The design strategy in utilizing GC-OMe<sup>2-</sup> is analogous to one which we have reported before (see Inorg. Chem. 2009, 48, 5620 and Inorg. Chem. 2010, 49, 7080) wherein Ni-SOD<sub>red</sub> active site mimics can be constructed at will with electronically variant RS<sup>-</sup> ligands. Discussed herein is the first account pertaining to the aqueous behavior of isolable, small molecule Ni-SOD model complexes (non-maquette based). Spectroscopic (FTIR, UV-vis, XAS) and electrochemical (CV) measurements suggest that 2-5 successfully simulate many of the electronic features of the Ni-SOD<sub>red</sub> active site but also reveal, in conjunction with <sup>1</sup>H NMR and ESI-MS studies, that these models are dynamic species with regards to RS<sup>-</sup> lability and bridging interactions in aqueous media suggesting a stabilizing role brought about by the protein architecture.

#### Introduction

The cytotoxic superoxide anion radical ( $O_2^{\bullet-}$ ) is an inevitable byproduct of aerobic metabolism that is capable of effecting significant cellular damage if not tightly regulated. In fact, increased production of superoxide has been associated with carcinogenesis, In fact, increased production of superoxide has been associated with carcinogenesis, In fact, increased production of superoxide has been associated with carcinogenesis, In fact, increased production of superoxide diseases such as Parkinson's In fact, increased production of an intracellular  $O_2^{\bullet-}$  ( $\sim 10^{-10}$  M), aerobic organisms employ superoxide dismutases (SODs), enzymes that catalyze the diffusion controlled ( $O_2^{\bullet-}$  to  $O_2^{\bullet-}$  and  $O_2^{\bullet-}$  to  $O_2^{\bullet-}$  and  $O_2^{\bullet-}$  to  $O_2^{\bullet-}$  and  $O_2^{\bullet-}$  to  $O_2^{\bullet-}$  and  $O_2^{\bullet-}$  are disproportionation reaction via toggling between oxidized and reduced states as

demonstrated in Scheme 1. Over the years, a rich knowledge of SODs employing redoxactive Fe,  $^{11-12}$  Mn,  $^{13}$  and Cu $^{14}$  has accumulated. However, less is understood about the newly discovered Ni-SOD,  $^{15-16}$  isolated from certain *Streptomyces* microbial strains and cyanobacteria.

The Ni-SOD enzyme is strikingly different from other known SODs. Crystallographic characterization reveals the Ni ion within a nine residue (HCDLPCGVY) "Ni-hook motif." In its reduced Ni(II) state, the metal is bound by the N-terminal amine of His1, the anionic carboxamido-N from Cys2, and the cysteine thiolates of Cys2 and Cys6 to complete an  $N_2S_2$  square-planar geometry (Chart 1). $^{17-18}$  In its oxidized Ni(III) state, the coordination geometry is square pyramidal with the imidazole-N of His1 occupying the apical position (Chart 1). $^{17-18}$  Although a growing body of protein, $^{15-16,19-25}$  polypeptide maquette $^{26-33}$  and small molecule  $^{34-40}$  literature has shed some light upon the role of this unusual donor set, many outstanding questions remain as to the interplay between the Ni ion, ligands, secondary coordination sphere, substrate and products during SOD catalysis. $^{19-29,34-38,41-43}$ 

While several redox-active Ni containing enzymes are currently known, <sup>44–48</sup> coordination of cysteine thiolates appears to be a reoccurring feature, presumably in order to depress the redox couples required to achieve both high Ni(III) and low Ni(I) oxidation states toward physiologically-accessible potentials. <sup>49–50</sup> Intriguingly, the majority of these enzymes catalyze reactions of great environmental and economical importance, such as the equilibration of CO<sub>2</sub> and CO for utilization as one-carbon equivalents <sup>46</sup> and the consumption and generation of H<sup>+</sup> and H<sub>2</sub>. <sup>44</sup> In NiFe-hydrogenase and Ni-SOD, the thiolate ligands have been implicated as active players in the catalytic cycle performing roles beyond redox modulation; in particular, H<sup>+</sup> storage and transport. <sup>25,51–53</sup> The unusual assembly of the Ni-SOD active site provides a new and unique opportunity to understand the effects imparted by electronic modifications of thiolate ligands while holding all other variables constant. This fundamental role of the atypical donor set, in conjunction with the obvious relevance of SOD to health and medicine, <sup>4–9</sup> has provided motivation for modeling studies pertaining to this unique metalloenzyme.

Previously, we reported a general and facile route toward Ni-SOD $_{red}$  model complexes utilizing the tridentate  $N_2S$  ligand  $nmp^{2-}$  (where  $nmp^{2-}$  is the dianion of N-(2-mercaptoethyl)picolinamide) that models the basal plane contributions of His1 and  $Cys2.^{37-38}$  The exogenously added thiolate ligand in these  $[Ni(nmp)(SR)]^-$  complexes (where  $RS^-$  models Cys6) can be systematically substituted via a variety of synthetic protocols. This feature was exploited to obtain a library of  $[Ni(nmp)(SR)]^-$  mimics with electronically variant monodentate thiolates which incorporate second-sphere functionalities tethered via the exogenously added thiolate. This study was fruitful in that it allowed for an in-depth analysis as to the effects manifested by intramolecular hydrogen bonding/thiolate protonation on the structural, spectroscopic, and reactivity properties of  $NiN_2S_2$  complexes related to Ni- $SOD_{red}$ . For example, we demonstrated that H-bonding to Ni-coordinated thiolates promotes more metal-based reactivity via reduction of S-contributions to the HOMO (relative to Ni) by decreasing the electrostatic potentials of the coordinated thiolates.  $^{37}$  Unfortunately, the [Ni(nmp)] series of complexes suffer from both poor solubility and stability in aqueous solution thus limiting reactivity studies to organic media.

The objective of the present work was to prepare small molecule  $[Ni(N_2S)(SR)]^-$  complexes of variant RS<sup>-</sup> (similar to the Ni(nmp) work) as Ni-SOD models that could be studied in a biologically-relevant aqueous environment. To this end, we utilized the dipeptide  $N_2S$  ligand,  $H_2N$ -Gly-L-Cys-OMe (abbreviated as GC-OMe $H_2$ , where H represents dissociable protons), as a suitable water-soluble construct to prepare the dinuclear metallosynthon,  $[Ni_2(GC\text{-OMe})_2]$  (1). Complex 1 was then used as a direct precursor towards the following

Ni-SOD model complexes:  $K[Ni(GC-OMe)(SC_6H_4-p-Cl)]$  (2), K[Ni(GC-OMe)(S'Bu)] (3),  $K[Ni(GC-OMe)(SC_6H_4-p-OMe)]$  (4), and K[Ni(GC-OMe)(S-NAc)] (5) (Chart 1). These monomeric Ni(II) complexes were prepared via methodologies previously described by us.  $^{37-38}$  The present study is the first regarding the characterization of discrete isolable Ni-SOD analogues in an aqueous environment (low MW containing only one peptide linkage; non-maquette based) providing for the use of small-molecule characterization techniques in aqueous media, which has until now been utilized exclusively for tripeptide  $^{32-33}$  and polypeptide maquette Ni-SOD analogues.  $^{26-29}$  The synthesis and properties of 2–5 are discussed below; the results obtained shed light on the behavior of species electronically analogous to the Ni-SOD<sub>red</sub> active site under pseudo-physiological conditions when stripped of their macromolecular surroundings.

## **Experimental Section**

#### **General Information**

All reagents were purchased from commercial suppliers and used as received unless otherwise noted. Acetonitrile (MeCN), methylene chloride (CH<sub>2</sub>Cl<sub>2</sub>), tetrahydrofuran (THF), diethyl ether (Et<sub>2</sub>O) and pentane were purified by passage through activated alumina columns using an MBraun MB-SPS solvent purification system and stored under a dinitrogen (N<sub>2</sub>) atmosphere before use. *N,N*-dimethylformamide (DMF) was purified with a VAC Solvent Purifier containing 4 Å molecular sieves and stored under similar conditions. Triethylamine (TEA) was dried over Na<sub>2</sub>SO<sub>3</sub>. Anhydrous MeOH was obtained by distilling from Mg(OMe)<sub>2</sub> under an N<sub>2</sub> atmosphere. All reactions were performed under an inert atmosphere of N<sub>2</sub> using standard Schlenk line techniques or in an MBraun Unilab glovebox under an atmosphere of purified N<sub>2</sub>. Potassium salts of the monodentate thiolate ligands were prepared according to a modified literature procedure<sup>54</sup> via addition of one mol-equiv of K(0) to the appropriate thiol in dry MeOH.

## **Physical Methods**

FTIR spectra were collected on a ThermoNicolet 6700 spectrophotometer running the OMNIC software; samples were prepared as pressed KBr pellets. Electronic absorption spectra were run at 298 K using a Cary-50 spectrophotometer containing a Quantum Northwest TC 125 temperature control unit. The UV-vis samples were prepared in gas-tight Teflon-lined screw cap quartz cells equipped with a rubber septum and an optical pathlength of 1 cm. Cyclic voltammetry measurements were performed with a PAR Model 273A potentiostat using a Ag/Ag<sup>+</sup> (0.01 M AgNO<sub>3</sub>/ 0.1 M <sup>n</sup>Bu<sub>4</sub>NPF<sub>6</sub> in MeCN) reference electrode, Pt counter electrode, and a Glassy Carbon milielectrode (2 mm) as the working electrode when using DMF. An Ag/AgCl reference electrode was used for aqueous samples. Measurements were performed at ambient temperature using 5.0 mM analyte in the appropriate solvent under Ar containing 0.1 M "Bu<sub>4</sub>NPF<sub>6</sub> as the supporting electrolyte in DMF or 0.5 M KNO<sub>3</sub> for aqueous measurements. The "Maximize Stability" mode was utilized in the PAR PowerCV software utilizing a low-pass 5.3 Hz filter. To ensure accuracy in the measured CVs, these experiments were performed in triplicate while polishing the working electrode between each run and we report an average  $E_{ox}$ . Additionally, potentials were checked and corrected by recording the CV of a ferrocene standard in DMF or a potassium ferricyanide standard in aqueous conditions (referenced to the ferro/ferricyanide couple in 50 mM pH 7.0 phosphate)<sup>55</sup> under the same experimental conditions as the complexes before each run. NMR spectra were recorded in the listed deuterated solvent on a 400 MHz Bruker BZH 400/52 NMR Spectrometer or 500 MHz Varian Unity INOVA NMR spectrometer at ambient temperature with chemical shifts referenced to TMS or residual protio signal of the deuterated solvent. Low resolution ESI-MS data were collected using a Perkin Elmer Sciex API I Plus quadrupole mass spectrometer and high resolution ESI-MS

data were collected using a Bruker Daltonics 9.4 T APEX Qh FT-ICR-MS. Elemental analysis for C, H, and N was performed at QTI-Intertek in Whitehouse, NJ.

## Synthesis of H<sub>2</sub>N-Gly-L-Cys-OMe•TFA (GC-OMe•TFA)

The synthesis of the ligand comprised the following steps:

Step 1. H<sub>2</sub>N-L-Cys(STrit)-OMe. To a batch of 13.701 g (52.629 mmol) of triphenyl methanol dissolved in 50 mL of trifluoroacetic acid (TFA) was added 9.095 g (52.99 mmol) of L-cysteine methyl ester hydrochloride forming a red-orange solution. The resultant solution was left to stir at RT for 1 h before it was concentrated to an orange oil, which was partitioned between 300 mL of CH<sub>2</sub>Cl<sub>2</sub> and 300 mL of H<sub>2</sub>O, resulting in bleaching of the orange color. Portions of K<sub>2</sub>CO<sub>3</sub> were then slowly added to the aqueous layer until a basic pH sustained for up to 1 h. The organic layer was then separated, washed with satd. NaHCO<sub>3</sub>(aq) and brine, dried over MgSO<sub>4</sub>, and concentrated to a pale oil which solidified after overnight stirring in hexanes. The white solids thus obtained were isolated via vacuum filtration (16.104 g, 42.660 mmol, 81%). mp: 57–58 °C. <sup>1</sup>H NMR (400 MHz, CDCl<sub>3</sub>, δ from TMS): 7.48 (d, 6H), 7.32 (t, 6H), 7.25 (t, 3H), 3.68 (s, 3H), 3.24 (m, 1H), 2.64 (dd, 1H), 2.52 (dd, 1H), 1.54 (br, s, 2H, NH<sub>2</sub>). <sup>13</sup>C NMR (100.6 MHz, CDCl<sub>3</sub>, δ from TMS): 174.26 (*C*=O), 144.64, 129.67, 128.03, 127.27-expand, 126.86, 66.94, 53.89, 52.22, 37.01. FTIR (KBr pellet),  $v_{max}$ (cm<sup>-1</sup>): 3391 (m, N-H), 3318 (w, N-H), 3062 (w), 2997 (w), 2966 (w), 2948 (w), 2920 (w), 1725 (vs, C=O<sub>ester</sub>), 1593 (m), 1487 (s), 1446 (s), 1434 (s), 1371 (m), 1348 (m), 1316 (m), 1260 (m), 1205 (s), 1186 (s), 1172 (s), 1095 (m), 1031 (m), 1020 (m), 1001 (m), 952 (m), 892 (w), 854 (m), 838 (m), 810 (m), 771 (m), 747 (s), 705 (s), 676 (m), 665 (m), 630 (m), 615 (s), 530 (w), 508 (m), 494 (m), 474 (m). LRMS-ESI (m/z): [M + H]<sup>+</sup> calcd for  $C_{23}H_{24}NO_2S$ , 378.2; found, 378.2.

**Step 2. Boc-Gly-L-Cys(STrit)-OMe**. A batch of 4.089 g (10.83 mmol) of H<sub>2</sub>N-L-Cys(STrit)-OMe and 2.947 g (10.82 mmol) of Boc-Gly-OSu were combined in 200 mL of CH<sub>2</sub>Cl<sub>2</sub> and stirred at RT overnight. The solution was then washed with satd. NaHCO<sub>3</sub>(aq) and brine, and dried over MgSO<sub>4</sub> before concentration to a white foam solid (4.934 g, 9.228 mmol, 85%). mp: 59–62 °C.  $^{1}$ H NMR (400 MHz, CDCl<sub>3</sub>, δ from TMS): 7.44 (d, 6H), 7.33 (t, 6H), 7.26 (t, 3H), 6.80 (br, s, 1H, N $H_{\text{peptide}}$ ), 5.38 (br, s, 1H, N $H_{\text{carbamate}}$ ), 4.59 (m, 1H), 3.82 (m, 2H), 3.72 (s, 3H), 2.71 (m, 2H), 1.49 (s, 9H).  $^{13}$ C NMR (100.6 MHz, CDCl<sub>3</sub>, δ from TMS): 170.79 ( $^{C}$ =O<sub>ester</sub>), 169.39 ( $^{C}$ =O<sub>peptide</sub>), 156.03 ( $^{C}$ =O<sub>carbamate</sub>), 144.35, 129.59, 128.11, 127.00-expand, 80.19, 67.06, 52.72, 51.28, 33.75, 28.40. FTIR (KBr pellet), ν<sub>max</sub> (cm<sup>-1</sup>): 3320 (br, s, N-H), 3057 (m), 3030 (m), 2977 (s), 2952 (m), 2931 (m), 1746 (vs, C=O<sub>ester</sub>), 1720 (vs, C=O<sub>carbamate</sub>), 1689 (vs, C=O<sub>peptide</sub>), 1595 (w), 1514 (s), 1493 (s), 1434 (m), 1391 (w), 1367 (m), 1248 (m), 1210 (m), 1168 (s), 1083 (w), 1050 (m), 1031 (m), 1001 (w), 985 (w), 941 (w), 862 (w), 766 (m), 744 (s), 701 (s), 675 (m), 621 (m), 544 (w), 505 (w). LRMS-ESI ( $^{m}$ /z): [M + K]<sup>+</sup> calcd for C<sub>30</sub>H<sub>34</sub>KN<sub>2</sub>O<sub>5</sub>S, 573.2; found, 573.0.

**Step 3. H<sub>2</sub>N-Gly-L-Cys-OMe•TFA (GC-OMeH<sub>2</sub>•TFA)**. A batch of 3.748 g (7.010 mmol) of Boc-Gly-L-Cys(STrit)-OMe was dissolved in 40 mL of a 1:1 CH<sub>2</sub>Cl<sub>2</sub>/TFA solution resulting in a bright-yellow color. After 30 min, 1.092 g (9.391 mmol) of Et<sub>3</sub>SiH was added dropwise to the solution, which bleached the bright-yellow solution to a clear and pale-yellow color. After 90 min stirring, the solution was concentrated to ~50% of its original volume and the resulting insoluble triphenyl methane byproduct was filtered off and washed with TFA. The solution was then concentrated to a pale oil, which solidified upon stirring in Et<sub>2</sub>O (1.601 g, 5.228 mmol, 75%). mp: 74–77 °C. <sup>1</sup>H NMR (500 MHz, CD<sub>3</sub>CN,  $\delta$  from protio solvent): 7.86 (br, s, 3H, N*H*<sub>3</sub>), 7.62 (s, N*H*<sub>peptide</sub>), 4.73 (m, 1H), 3.80 (m, 2H), 3.72 (s, 3H), 2.93 (m, 2H), 1.92 (br s, coincides with solvent protio signal thus difficult to integrate, S*H*). <sup>13</sup>C NMR (100.6 MHz,

CD<sub>3</sub>CN,  $\delta$  from solvent): 222.78 (*C*=O<sub>TFA</sub>), 171.45 (*C*=O<sub>ester</sub>), 167.52 (*C*=O<sub>peptide</sub>), 107.40 (*C*F<sub>3</sub>), 56.11, 53.64, 41.95, 31.47, 27.17-extra13C. <sup>1</sup>H NMR (500 MHz, D<sub>2</sub>O,  $\delta$  from protio solvent): 4.82 (m, 1H), 3.94 (s, 2H), 3.82 (s, 3H), 3.03 (m, 2H). FTIR (KBr pellet),  $\nu_{max}$  (cm<sup>-1</sup>): 3325 (m, NH), 3138 (br, w, NH), 1753 (s, C=O<sub>ester</sub>), 1677 (vs, C=O<sub>peptide</sub>), 1631 (w) 1563 (w), 1552 (m), 1536 (w), 1513 (w), 1493 (w), 1434 (m), 1350 (m), 1323 (w), 1208 (s, C-F), 1186 (s, C-F), 1129 (s), 1043 (w), 965 (w), 906 (m), 841 (m), 802 (m), 726 (m), 572 (w). LRMS-ESI (*m/z*): [M + H]<sup>+</sup> calcd for C<sub>6</sub>H<sub>13</sub>N<sub>2</sub>O<sub>3</sub>S, 193.2; found, 193.0.

## [Ni<sub>2</sub>(GC-OMe)<sub>2</sub>](1)

Procedure 1 (TFA adduct)—To a batch of 0.174 g (0.699 mmol) of Ni(OAc)<sub>2</sub>•4H<sub>2</sub>O stirring in 12 mL of MeOH was added a 4 mL MeOH solution of GC-OMeH2•TFA (0.217 g, 0.709 mmol) followed by a 3 mL MeOH soltion of NaOAc (0.060 g, 0.731 mmol). The resultant deep orange solution was stirred at RT for 16 h after which the reaction was concentrated to dryness to afford an orange residue. This residue was then stirried in 20 mL of MeCN, which resulted in 0.153 g (0.250 mmol, 72%) of product as peach colored solids. <sup>1</sup>H NMR (400 MHz, D<sub>2</sub>O, δ from solvent): 4.28 (m, 1H), 3.96 (s, 3H), 3.49 (d, 1H), 3.32 (d, 1H)-dofd, 2.51 (br, s, 1H), 2.31 (d, 1H), 2.08 (s, 1H), 1.94 (s, 1H). FTIR (KBr pellet),  $v_{\text{max}}$  (cm<sup>-1</sup>): 3420 (w, br, OH), 3246 (m, br, N-H), 3119 (m, br, N-H), 2950 (w), 1729 (s, C=O<sub>ester</sub>), 1694 (m, C=O<sub>TFA</sub>), 1601 (vs, C=O<sub>peptide</sub>), 1437 (m), 1409 (s), 1338 (w), 1273 (w), 1205 (s, C-F), 1169 (s, C-F), 1138 (m), 1019 (w), 973 (w), 944 (w), 843 (w), 801 (w), 722 (w), 669 (w), 650 (w), 625 (w), 584 (w), 459 (w). HRMS-ESI (m/z):  $[M + H]^+$ calcd for C<sub>12</sub>H<sub>21</sub>N<sub>4</sub>Ni<sub>2</sub>O<sub>6</sub>S<sub>2</sub> (relative abundance), 496.9604 (100), 497.9637 (13), 498.9559 (76), 499.9591 (10), 500.9547 (15); Found, 496.9614 (100), 497.9646 (11), 498.9570 (88), 499.9604 (10), 500.9522 (18). UV-vis (pH 7.5, 50 mM PIPES, 298 K)  $\lambda_{max}$ , nm ( $\epsilon$ , M<sup>-1</sup> cm<sup>-1</sup>): 338 (4,470), 458 (560). Anal. Calcd for C<sub>12</sub>H<sub>20</sub>N<sub>4</sub>Ni<sub>2</sub>O<sub>6</sub>S<sub>2</sub>•TFA•2H<sub>2</sub>O: C, 25.95; H, 3.89; N, 8.65. Found: C, 26.13; H, 3.94; N, 8.62.

**Procedure 2**—To a batch of 1.292 g (5.192 mmol) of Ni(OAc)<sub>2</sub>•4H<sub>2</sub>O and 0.428 g (5.22 mmol) of NaOAc dissolved in 80 mL of MeOH was added 1.584 g (5.172 mmol) of GC-OMeH<sub>2</sub>•TFA in 10 mL of MeOH. The reaction mixture instantly became a deep red-orange color upon addition of ligand and was subsequently heated to 50 °C for 16 h, which resulted in the precipitation of product as pink solids. The solids were isolated via vacuum filtration to afford 1.100 g (2.210 mmol, 85%) of product. The isolated product is not readily soluble as is the TFA-adduct (see above), but prolonged stirring in D<sub>2</sub>O or buffer provided orange solutions with identical spectral properties ( $^{1}$ H NMR, UV-vis, ESI-MS). FTIR reveled no TFA peaks. FTIR (KBr pellet),  $\nu_{max}$  (cm<sup>-1</sup>): 3326 (w, N-H), 3228 (w, N-H), 3084 (br w, N-H), 2978 (w), 2962 (w), 2929 (w), 1755 (s, C=O<sub>ester</sub>), 1578 (vs, C=O<sub>peptide</sub>), 1433 (m), 1404 (m), 1360 (m), 1312 (w), 1265 (w), 1200 (m), 1177 (m), 1150 (m), 1114 (m), 1055 (w), 1030 (w), 993 (w), 969 (w), 946 (w), 853 (w), 801 (w), 717 (w), 660 (w), 603 (w), 573 (w), 483 (w), 424 (m). Anal. Calcd for C<sub>12</sub>H<sub>20</sub>N<sub>4</sub>Ni<sub>2</sub>O<sub>6</sub>S<sub>2</sub>•0.5H<sub>2</sub>O: C, 28.44; H, 4.18; N, 11.05. Found: C, 28.47; H, 3.94; N, 10.78.

## [Ni<sub>2</sub>(GC-OMe)<sub>2</sub>] (1) prepared in situ

To a freshly dissolved batch of 18 mg (0.06 mmol) of GC-OMeH<sub>2</sub>•TFA in pH 7.5 buffer (50 mM PIPES), was added 15 mg (0.06 mmol) of Ni(OAc)<sub>2</sub>•4H<sub>2</sub>O to form a richly colored orange solution. All spectral properties are in accordance with those of solid batches of isolated 1 upon dissolution.

## $K[Ni(GC-OMe)(SC_6H_4-p-CI)]$ (2)

To an 8 mL DMF solution containing 0.142 g (0.777 mmol) of KSC<sub>6</sub>H<sub>4</sub>-p-Cl was added a 5 mL DMF slurry of 1 (0.202 g, 0.406 mmol). The resulting purple heterogeneous mixture was heated to 45 °C and stirred at this temperature for 16 h to form a rich mostly homogeneous violet colored solution. The reaction was subsequently cooled to RT, filtered to remove any unreacted 1, and the violet mother liquor was concentrated to dryness. The resultant purple residue was then taken up in 2 mL of THF, which was then precipiated out by addition of 12 mL of Et<sub>2</sub>O. The product was collected as dull violet solids via vacuum filtration (0.316 g, 0.732 mmol, 94%). <sup>1</sup>H NMR (500 MHz, D<sub>2</sub>O, as isolated product in the presence of one extra mol-equiv of KSC<sub>6</sub>H<sub>4</sub>-p-Cl, δ from protio solvent): 7.53 (d, 1.4H), 7.30 (d, 1.7H, free  $KSC_6H_4$ -p-Cl), 7.14 (d, 1.4H), 7.08 (d, 1.7H, free  $KSC_6H_4$ -p-Cl), 4.15 (m, 1H), 3.79 (s, 3H), 3.31 (d, 1H), 3.15 (d, 1H)-dofd, 2.60 (m, 1H), 2.24 (d, 1H). <sup>1</sup>H NMR (400 MHz, CD<sub>3</sub>CN, as isolated solid, δ from protio solvent): 7.68 (d, 1.3H), 6.93 (d, 1.1H), 3.84 (m, 1H), 3.61 (s, 2.4H), 3.01 (m, 1H), 2.91 (m, 1H), 2.36 (m, 1H), 2.15 (s, 1H, NH), 2.13 (m, 1H), 1.87 (br s, 1H, NH). FTIR (KBr pellet),  $v_{\text{max}}$  (cm<sup>-1</sup>): 3325 (w, NH), 3195 (br w, N-H), 3108 (br w, N-H), 2948 (m), 2924 (m), 1722 (s, C=O<sub>ester</sub>), 1586 (vs, C=O<sub>peptide</sub>), 1468 (s), 1437 (m), 1410 (m), 1336 (w), 1265 (w), 1207 (m), 1168 (m), 1090 (s), 1033 (m), 1010 (m), 934 (w), 818 (m), 740 (w), 701 (w), 662 (w), 543 (m), 499 (w), 425 (w). HRMS-ESI (m/z):  $[M - K]^-$  calcd for  $C_{12}H_{14}ClN_2NiO_3S_2$  (relative abundance), 390.9488 (100), 391.9521 (13), 392.9444 (48), 393.9478 (6), 394.9416 (21); Found, 390.9487 (100), 391.8209 (13), 392.9448 (69), 393.9479 (16), 394.9404 (21). UV-vis (DMF, 298 K)  $\lambda_{max}$ , nm ( $\epsilon$ , M<sup>-1</sup> cm<sup>-1</sup>): 481 (390), 560 (230). UV-vis (pH 7.5, 50 mM PIPES, 298 K)  $\lambda_{max}$ , nm  $(ε, M^{-1} cm^{-1})$ : 471 (430), 560 (240).  $E_{ox}$  (DMF): 220 mV.  $E_{ox}$  (pH 7.4): 285 mV. Anal. Calcd for C<sub>12</sub>H<sub>14</sub>ClKN<sub>2</sub>NiO<sub>3</sub>S<sub>2</sub>•0.5H<sub>2</sub>O: C, 32.71; H, 3.43; N, 6.36. Found: C, 32.63; H, 3.56; N, 6.50.

## $K[Ni(GC-OMe)(S^tBu)]$ (3)

To 115 µL (0.092 g, 1.02 mmol) of tert-butyl thiol dissolved in 3 mL of DMF was added 0.040 g (0.997 mmol) of KH as a 4 mL DMF slurry to generate KS'Bu. Immediate effervescence was observed and a pale yellow homogenous solution formed over the course of 20 min. To this soltion was added a 5 mL DMF slurry of 1 (0.278 g, 0.558 mmol) resulting in a purple heterogeneous mixture. This solution was then heated to 45 °C and stirred for 16 h to form a rich violet colored solution. The reaction was subsequently cooled to RT, filtered to remove any unreacted 1, and the violet mother liquor was concentrated to dryness. The resultant purple residue was taken up in 6 mL of THF, which was treated with 25 mL of Et<sub>2</sub>O to form free flowing solids. The product was collected as pink solids via vacuum filtration (0.328 g, 0.870 mmol, 87%). <sup>1</sup>H NMR (400 MHz, D<sub>2</sub>O, as isolated product in the presence of one extra mol-equiv of KS'Bu, δ from protio solvent): 4.01 (d, 1H), 3.71 (s, 3H), 3.30 (d, 1H), 3.14 (d, 1H)dofd?, 2.53 (m, 1H), 2.21 (d 1H), 1.26 (s, 9H). <sup>1</sup>H NMR (500 MHz, CD<sub>3</sub>CN, as isolated solid?, δ from protio solvent): 3.70 (m, 1H), 3.59 (s, 3H), 3.04 (m, 1H), 2.95 (m, 1H), 2.30 (m, 1H), 2.13 (m, 1H), 1.84 (s, 2H, NH), 1.31 (s, 9H). FTIR (KBr pellet),  $v_{max}$  (cm<sup>-1</sup>): 3343 (br w, N-H), 3222 (br w, N-H), 3107 (br w, N-H), 2948 (w), 2887 (w), 2848 (w), 1721 (m, C=O<sub>ester</sub>), 1584 (vs, C=O<sub>peptide</sub>), 1439 (w), 1410 (m), 1355 (w), 1273 (w), 1207 (m), 1166 (m), 932 (w), 742 (w), 646 (w), 586 (w), 465 (w). UV-vis (DMF, 298 K)  $\lambda_{\text{max}}$ , nm (e, M<sup>-1</sup> cm<sup>-1</sup>): 358 (1410), 484 (350), 570 (230).  $E_{\text{ox}}$ (DMF): 80 mV. Anal. Calcd for C<sub>10</sub>H<sub>19</sub>KN<sub>2</sub>NiO<sub>3</sub>S<sub>2</sub>•1.2H<sub>2</sub>O: C, 30.39; H, 5.36; N, 7.09. Found: C, 30.08; H, 5.02; N, 7.16.

#### $K[Ni(GC-OMe)(SC_6H_4-p-OMe)]$ (4)

To a 3 mL DMF solution containing 0.046 g (0.258 mmol) of  $KSC_6H_4$ -p-OMe was added a 3 mL DMF slurry of **1** (0.073 g, 0.147 mmol). The purple heterogeneous reaction mixture

that formed was then heated to 45 °C and stirred for 16 h to form a violet-brown mostly homogeneous solution. The reaction was subsequently cooled to RT, filtered to remove any unreacted 1, and the violet-brown mother liquor was concentrated to dryness. To the resultant red-brown residue was added 5 mL each of THF and Et<sub>2</sub>O and the residue was scraped to form free flowing solids. The product was collected as red-brown solids via vacuum filtration (0.096 g, 0.225 mmol, 87% yield). <sup>1</sup>H NMR (400 MHz, D<sub>2</sub>O, as isolated product in the presence of one extra mol-equiv of KSC<sub>6</sub> $H_4$ -p-OMe,  $\delta$  from protio solvent): 7.37 (d, 2H), 7.21 (d, 2H, free  $KSC_6H_4$ -p-OMe), 6.72 (m, 4H, overlap of bound and free KSC<sub>6</sub>H<sub>4</sub>-p-OMe), 4.08 (d, 1H), 3.71 (s, 9H, coincidental peaks from: 3H from OMe of coordinated KSC<sub>6</sub>H<sub>4</sub>-p-OMe, 3H from OMe of free KSC<sub>6</sub>H<sub>4</sub>-p-OMe), 3.23 (m, 1H), 3.07 (m, 1H)-dofd?, 2.53 (m, 2H). <sup>1</sup>H NMR (500 MHz, CD<sub>3</sub>CN, as isolated solid?, δ from protio solvent): 7.40 (d, 2H), 6.50 (d, 0.3H), 6.41 (d, 1.7H), 3.75 (t, 1H), 3.55 (s, 3H), 3.44 (s, 3H), 2.93 (m, 2H), 2.17 (m, 1H), 2.08 (m, 1H and br s, 1H, NH), 1.85 (br s, 1H, NH). FTIR (KBr pellet),  $v_{\text{max}}$  (cm<sup>-1</sup>): 3319 (w, N-H), 3190 (br w, N-H), 3090 (br w, N-H), 2946 (w), 2834 (w), 1720 (s, C=O<sub>ester</sub>), 1663 (m, C=O<sub>DMF</sub>), 1587 (vs, C=O<sub>peptide</sub>), 1486 (s), 1463 (w), 1439 (m), 1409 (m), 1336 (w), 1273 (m), 1235 (s), 1169 (s), 1099 (m), 1028 (m), 933 (w), 826 (w), 796 (w), 638 (w), 625 (w), 561 (w), 525 (w), 470 (w), 425 (w). HRMS-ESI (m/z): [M – K]<sup>-</sup> calcd for  $C_{13}H_{17}N_2NiO_4S_2$  (relative abundance), 386.9983 (100), 388.0017 (14), 388.9940 (48), 389.9973 (7); Found, 386.9980 (100), 388.0011 (14), 388.9936 (46), 389.9983 (11). UV-vis (DMF, 298 K)  $\lambda_{\text{max}}$ , nm ( $\epsilon$ , M<sup>-1</sup> cm<sup>-1</sup>): 480 (510), 565 (250). UVvis (pH 7.5, 50 mM PIPES, 298 K)  $\lambda_{\text{max}}$ , nm ( $\epsilon$ , M<sup>-1</sup> cm<sup>-1</sup>): 467 (420), 550 (230).  $E_{\text{ox}}$ (DMF): 170 mV. E<sub>ox</sub> (pH 7.4): 315 mV. Anal. Calcd for C<sub>13</sub>H<sub>17</sub>KN<sub>2</sub>NiO<sub>4</sub>S<sub>2</sub>•0.5H<sub>2</sub>O: C, 35.79; H, 4.16; N, 6.42. Found: C, 35.84; H, 4.46; N, 6.48.

#### K[Ni(GC-OMe)(S-NAc)] (5)

To a 5 mL DMF solution containing 0.094 g (0.249 mmol) of 3 was added a 2 mL DMF solution of N-acetyl-L-cysteine methyl ester (0.045 g, 0.254 mmol). The solution rapidly changed from violet to orange-brown and was left to stir at RT for 16 h. The solution was then concentrated to a brick-red colored residue and stirred in 15 mL of a 2:1 Et<sub>2</sub>O/THF mixture to afford free flowing solids. The solids were collected via vacuum filtration to yield 0.105 g (0.226 mmol, 91% yield) of product. <sup>1</sup>H NMR (400 MHz, D<sub>2</sub>O, as isolated product in the presence of one extra mol-equiv of KS-NAc, δ from protio solvent): 4.45 (t, 1H, free KS-NAc), 4.32 (t, 1H), 4.11 (d, 1H), 3.73 (s, 6H, coincidental peaks: 3H each from OMe of coordinated [GC-OMe]<sup>2-</sup> and [S-NAc]<sup>-</sup>, 3H from OMe of free KS-NAc), 3.31 (d, 1H), 3.17 (d, 1H)-dofd?, 2.86 (m, 2.5H, free KS-NAc), 2.63 (m, 1H), 2.26 (d, 1H), 2.14 (m, 2H), 2.08 (s, 3H), 2.02 (s, 4H, free KS-NAc). <sup>1</sup>H NMR (500 MHz, CD<sub>3</sub>CN, as isolated solid?, δ from protio solvent): 8.62 (br s, 1H, NH), 4.05 (br s, 1H), 3.90 (br s, 1H), 3.60 (s, 8H, coincidental peaks from: OMe of both coordinated [GC-OMe]<sup>2-</sup> and [SN-Ac]<sup>-</sup>, residual THF from reaction workup), 3.32 (br s, 1H), 3.05 (m, 1H), 2.97 (m, 1H), 2.51 (m, 1H), 2.14 (m, 10H, integrates slightly high due to overlap with residual H<sub>2</sub>O peak). FTIR (KBr pellet),  $v_{\text{max}}$  (cm<sup>-1</sup>): 3246 (br w, N-H), 2950 (w), 2919 (w), 2848 (w), 1731 (s, C=O\_{\text{ester}}), 1662 (s, C=O<sub>SNAC peptide</sub>), 1589 (vs, C=O<sub>GCOMe peptide</sub>), 1436 (m), 1412 (m), 1372 (w), 1337 (w), 1302 (w), 1268 (w), 1212 (m), 1167 (m), 1122 (w), 1032 (w), 938 (w), 901 (w), 843 (w), 800 (w), 661 (w), 567 (w), 488 (w), 423 (w). HRMS-ESI (m/z): [M – K]<sup>-</sup> calcd for  $C_{12}H_{20}N_3NiO_6S_2$  (relative abundance), 424.0147 (100), 425.0181 (13), 426.0103 (48), 427.0137 (6), 428.0077 (5); Found, 424.0144 (100), 425.0180 (12), 426.0101 (48), 427.0135 (6), 428.0081 (4). LRMS-ESI (m/z):  $[M - K]^-$  calcd for  $C_{12}H_{20}N_3NiO_6S_2$ , 424.0; found, 424.0. UV-vis (DMF, 298 K)  $\lambda_{\text{max}}$ , nm (e, M<sup>-1</sup> cm<sup>-1</sup>): 358 sh (1,230), 463 (350), 545 (160). UV-vis (pH 7.5, 50 mM PIPES, 298 K)  $\lambda_{\text{max}}$ , nm ( $\epsilon$ , M<sup>-1</sup> cm<sup>-1</sup>): 334 (1,210), 463 (300), 545 (140).  $E_{\rm ox}$  (DMF): 310 mV.  $E_{\rm ox}$  (pH 7.4): 550 mV. Anal. calcd for C<sub>12</sub>H<sub>20</sub>KN<sub>3</sub>NiO<sub>6</sub>S<sub>2</sub>•0.33THF•0.33H<sub>2</sub>O: C, 32.40; H, 4.76; N, 8.50. Found: C, 32.46; H, 4.80; N, 8.67.

#### Bulk oxidation of 2

To a batch of 52 mg (0.12 mmol) of  $\bf 2$  in 3 mL of DMF was added 40 mg (0.12 mmol) of ferrocenium hexafluorophosphate in 3 mL of DMF. Instantantaneously, the violet solution developed an orange-brown color and was left to stir at RT for 2 h. The reaction mixture was then concentrated to an orange-brown residue, which solidified upon stirring in Et<sub>2</sub>O. Brown solids (45 mg) were separated via vacuum filtration and the yellow mother liquor was concentrated to a pale yellow residue (40 mg). FTIR (KBr),  $^1$ H NMR (D<sub>2</sub>O), and ESI-MS (positive ion mode) revealed the brown insoluble solids to be comprised of  $\bf 1$  and KPF<sub>6</sub> (87% recovery) while  $^1$ H NMR in CDCl<sub>3</sub> of the yellow Et<sub>2</sub>O-soluble residue to be comprised solely of ferrocene and the disulfide of the thiol HSC<sub>6</sub>H<sub>4</sub>-p-Cl (100% recovery).

#### X-ray Absorption Studies

Samples were loaded under anaerobic conditions into 0.5 mm thick XAS aluminum sample holders with Mylar-tape windows and quickly frozen in liquid nitrogen prior to XAS data collection. Nickel K-edge XAS data were collected at Stanford Synchrotron Radiation Lightsource (SSRL) on beamline 7–3 with the SPEAR storage ring operating at 3.0 GeV, 345–350 mA. X-ray absorption spectra for the solid samples were recorded with the sample at 10 K using a 1 mm × 4 mm vertically aperture beam incident on a fully tuned Si[220] double-crystal monochromator, and collected using transmission mode. Three ionization chambers with  $N_2$  gas were used, with the first defining  $I_0$ . A nickel foil was placed between the second and third ionization chambers  $I_1$  and  $I_2$  to serve as an internal calibration standard, with the first inflection point for the nickel foil assigned at 8331.6 eV. k values were calculated using a threshold (k = 0) energy of 8340 eV. The averaged XAS data for a solid sample represent 5-6 scans, each of 27 minutes duration; the averaged spectra were calculated as  $log(I_0/I_1)$ . Data reduction and analysis were performed with EXAFSPAK software (www-ssrl.slac.stanford.edu/exafspak.html) according to standard procedures as described before. <sup>56</sup> Fourier transforms of the EXAFS spectra were generated using sulfurbased phase correction. Phase and amplitude functions used in the curve fitting were calculated using FEFF version 8.0.

#### **Results and Discussion**

#### **Synthesis**

In constructing accurate structural and functional models of Ni-SOD, certain design elements must be considered. First, the ligand frame must contain a mixed N/S donor set to mimic the coordination sphere observed in the enzyme. Second, and beyond a mere stoichiometric replication of the donor atoms, is the electronic nature of the N/S frame which should contain one peptide-N (anionic peptide nitrogens typically referred to as carboxamides), one primary amine-N, and two cis-thiolates situated in a planar N<sub>2</sub>S<sub>2</sub> arrangement. An additional imidazole-N ligand would be required to replicate the fourcoordinate-to-five-coordinate Ni(II/III)-SOD redox conversion. Third, the ligand construct should be amenable to a variety of straightforward modifications to allow for at will electronic and structural modifications to "fine tune" the biomimetic for its desirable function. Several groups have achieved some or all of these criteria by employing: (i) small peptides or peptide maquettes typically three-to-twelve amino acids long; 26-29,32-33 (ii) symmetric N<sub>2</sub>S<sub>2</sub> frames that approximate the electronic nature of the Ni-SOD donors;<sup>39–40,57</sup> (iii) electronically accurate N<sub>2</sub>S<sub>2</sub> frames;<sup>34–35</sup> (iv) asymmetric N<sub>2</sub>S ligands that approximate the Ni active site with an open coordination site where exogenous Ndonors bind (NiN<sub>3</sub>S);<sup>58–59</sup> and (v) asymmetric N<sub>2</sub>S ligands with Ni-SOD accurate donors with an open coordination site where exogenous S-ligands bind to afford NiN<sub>2</sub>S<sub>2</sub> species. <sup>37–38</sup> In this work we utilized design methodologies from i and v (see previous) resulting in the Gly-Cys N<sub>2</sub>S ligand that we denote as GC-OMeH<sub>2</sub> (where H represents

dissociable protons). We hypothesized that  $GC\text{-}OMeH_2$  would provide a water soluble small molecule Ni-SOD biomimetic that models the *exact contributions* of His1 and Cys2 in the enzyme. Simultaneously, in a strategy developed by our group, a fourth and exchangeable coordination site amenable to synthetic fine tuning is left available by which monodentate thiolate ligands (modeling the Cys6 contribution of Ni-SOD) can be appended.

The synthesis of GC-OMeH $_2$  occurs in three steps by standard peptide coupling routes that afford the final ligand in high yield (Scheme 1). Protection of the thiol group of L-cysteine methyl ester occurs in 81% yield by reaction of the amino acid with triphenyl methanol (trityl-protection) in TFA. Formation of the pre-ligand is achieved by coupling of the protected cysteine methyl ester with BOC-Gly-OSu resulting in the S-trityl protected ligand in 85% yield. Finally, deprotection of the trityl and BOC groups with Et $_3$ SiH in a TFA/ CH $_2$ Cl $_2$  (1:1) mixture furnished the TFA-adduct of GC-OMeH $_2$  in 74% yield. The ligand is a white solid material that is thermally stable even in aerobic conditions.

The monomeric Ni(II)-N<sub>2</sub>S<sub>2</sub> complexes originate from the dimeric species, [Ni<sub>2</sub>(GC-OMe)<sub>2</sub>] (1), which is isolated in high yield by reaction of Ni(OAc)<sub>2</sub>•4H<sub>2</sub>O with ligand and one mol-equiv of NaOAc in MeOH at RT resulting in orange-colored solutions. TFA still seems to be associated with 1 depending on the reaction conditions, which has been confirmed by FTIR and elemental analysis (see experimental section). These peach-colored solids have been formulated as an aquated TFA species, namely 1. TFA. 2H2O, according to microanalysis. Heating MeOH solutions of 1•TFA•2H<sub>2</sub>O to 50°C for 16 h resulted in the precipitation of analytically-pure [Ni<sub>2</sub>(GC-OMe)<sub>2</sub>] (1) as pink solids with no evidence of TFA peaks in its IR spectrum. Complex 1 is generally insoluble in both polar and non-polar solvents, a property consistent with previously isolated dimeric S,S-bridged Ni<sub>2</sub>(N<sub>2</sub>S)<sub>2</sub> complexes;<sup>37–38</sup> however, stirring in water resulted in slow dissolution to afford orange solutions with a spectral profile (vide infra) identical to that obtained via the spontaneous metallation of GC-OMeH<sub>2</sub>•TFA with Ni(II) in pH 7.5 PIPES buffer. ESI-MS<sup>+</sup> analysis of 1 also revealed the presence of species corresponding to  $[Ni_2(GC-OMe)_2 + H]^+ (1 + H)$ , [Ni<sub>3</sub>(GC-OMe)<sub>3</sub> + H]<sup>+</sup> and [Ni<sub>4</sub>GC-OMe)<sub>4</sub> + H]<sup>+</sup>, suggesting that various permutations of 1:1 Ni/GC-OMe stoichiometry may exist upon dissolution (Figures S17–19). Regardless, <sup>1</sup>H NMR studies in D<sub>2</sub>O revealed a chemical equivalency throughout any species which may be present (vide infra). It should be noted that deprotonation of ligand protons with a strong base such as NaH in an aprotic solvent (MeCN) resulted in the formation of intractable brown solids upon addition of Ni(II); the exact nature of such species is unknown at present, but FTIR reveals loss of the GC-OMeH2 ester functionality suggesting that the coordination chemistry of GC-OMeH2•TFA with Ni(II) is relatively facile in polar protic solvents and a strong base is not required.

Despite its unfavorable solubility properties, complex 1 is a good metallosynthon in the preparation of the monomeric Ni(II) complexes,  $K[Ni(GC-OMe)(SC_6H_4-p-Cl)]$  (2), K[Ni(GC-OMe)(S'Bu)] (3),  $K[Ni(GC-OMe)(SC_6H_4-p-OMe)]$  (4), and K[Ni(GC-OMe)(SNAc)] (5) via addition of two mol-equiv of the appropriate potassium thiolate salts to DMF solutions of 1 heated to 45 °C (Scheme 2) (where  $SC_6H_4-p-Cl =$  thiolate of *para*-chlorobenzene thiol; S'Bu = thiolate of *tert*-butylthiol;  $SC_6H_4-p-OMe =$  thiolate of *para*-methoxybenzenethiol; SNAc = thiolate of *N*-acetyl L-cysteine methyl ester). The  $S_5S'-$  bridge splitting reactions to form 2–4 resulted in high yields of the complexes (87–90%). As reported by our group, complexes of general formula  $[Ni(N_2S)(SR)]^-$  can be synthesized several ways: (i)  $S_5S'$ -bridge splitting of Ni dimers; (ii)  $pK_a$  driven thiol exchange; and (iii) a disulfide redox exchange procedure. These alternate methodologies have been successfully applied to this generation of water-soluble Ni-SOD mimics. For example, complex 5 was obtained in 90% yield via the addition of one mol-equiv of HSNAc to 3 in DMF. Complex 2 was also prepared from 3 utilizing 0.5 mol-equiv of the disulfide of

HSC<sub>6</sub>H<sub>4</sub>-*p*-Cl. These facile reactions to obtain monomeric Ni(II) species demonstrate the efficacy of these preparations when applied to different ligand systems that may be applied to future Ni-SOD models.

## **Properties**

#### General

Complexes **1–5** are stable in anaerobic aqueous solutions for up to 16 h as monitored by  $^1H$  NMR. No evidence of ligand protonation, dissociation, or metal-mediated ester hydrolysis is observed which is in contrast to other reported Ni(II)N<sub>2</sub>S<sub>2</sub> complexes.  $^{60}$  UV-vis spectral monitoring of complexes **2**, **4**, and **5** in pH 7.5 buffer (PIPES) revealed slight increases in the intensity of  $\lambda_{max}$  over prolonged time periods (> 6 h) due to light scattering as these solutions became cloudy. Similarly, the dimeric complex **1** is air stable in solution over 16 h as evidenced by  $^1H$  NMR and UV-vis consistent with the stability brought about by S,S'-bridging. Collectively, solutions of **2–5** are relatively air stable and can be handled aerobically without significant decomposition on the hour timescale. However, prolonged aerobic storage resulted in color-bleaching and cloudiness for periods of extended exposure (> 6 h).

#### Infrared

FTIR spectra of metal-peptide complexes serve as good indicators for peptido-N $\rightarrow$ M binding from the observed red-shift in  $\nu_{CO}$  of the carbonyl peptide. This noted shift is observed in **1–5** with  $\nu_{CO}$  frequencies between 1578 to 1589 cm<sup>-1</sup> (KBr matrix), which has red-shifted ~100 cm<sup>-1</sup> from the free ligand ( $\nu_{CO}$ : 1677 cm<sup>-1</sup> in KBr) and confirms formation of the peptido-N $\rightarrow$ M bond. In general,  $\nu_{CO}$  appears to be invariant, regardless of the donor strength of the monodentate thiolate ligand trans to the peptido-N. In fact, the lowest energy  $\nu_{CO}$  stretch belongs to **1** despite the bridging nature of the coordinated thiolates. As expected,  $\nu_{NH}$  of the peptide-N is absent in the Ni(II) complexes. Coordination of the -NH<sub>2</sub> functionality in **1–5** is also evident as the  $\nu_{NH}$  symmetric stretches appear at values as low as 3042 cm<sup>-1</sup> (**5**) to 3108 cm<sup>-1</sup> (**2**) compared to  $\nu_{NH}$  of the free ligand (3318 cm<sup>-1</sup>). In general,  $\nu_{NH}$  of organic primary amines occur at values 3250 cm<sup>-1</sup>.61

## <sup>1</sup>H NMR and ESI-MS

<sup>1</sup>H NMR of complexes 1–5 reveal that these Ni(II) complexes are  $a^8$  square-planar systems in solution (D<sub>2</sub>O and CD<sub>3</sub>CN at 298 K) as evident by the diamagnetic (S = 0) spectra. For example, the D<sub>2</sub>O <sup>1</sup>H NMR spectrum of dimer **1** revealed only one signal per nonequivalent proton, indicative of an electronically identical environment per Ni(II) with respect to GC-OMe<sup>2-</sup> protons. In contrast, the D<sub>2</sub>O <sup>1</sup>H NMR of as-isolated **2–5** display broad, ill-resolved signals indicative of an equilibrium mixture of Ni(II) species likely due to loss of the exogenous RS<sup>-</sup> ligand and formation of [Ni<sub>x</sub>(GC-OMe)<sub>x</sub>(SR)] or [Ni(GC-OMe) (OH<sub>2</sub>)<sub>x</sub>]-type species. The precise nature of the species present upon dissolution of the asisolated Ni(II) complexes 2-5 is unknown, but the spectra suggest more than one which may be oligomeric in nature. In fact, site-directed mutagenesis of the Cys-S ligands of Ni-SOD suggest that even mutation of one cysteine to serine promotes a high-spin (S = 1) octahedral Ni(II) site with no S-ligands (replaced by H<sub>2</sub>O).<sup>21,23</sup> When one mol-equiv of the corresponding thiolate is added to these D<sub>2</sub>O solutions, however, the NMR became wellresolved with defined peaks that are consistent with monomeric (S = 0) [Ni(GC-OMe) (SR)] complexes (Figure 1 for 2, Supporting Information for 3–5). Indeed, ESI-MS analysis of as-isolated 2 and 4 dissolved in protic solvents revealed ions corresponding to  $[Ni_2(GC-OMe)_2(SR)]^-$ ,  $[Ni_3(GC-OMe)_3(SR)]^-$  and  $[Ni_4(GC-OMe)_4(SR)]^-$  in addition to those of the parent ion (Figures S20–27). Similarly, [Ni<sub>2</sub>(GC-OMe)<sub>2</sub>(S-NAc)]<sup>-</sup>, is observed along with the parent ion for 5. The 'BuS' ligand of complex 3 dissociated completely in pH

7.5 buffer affording orange-colored solutions that are consistent with reformation of dimer 1. Addition of one mol-equiv of KS'Bu re-established the violet monomer (vide infra). Furthermore, neither parent ion 3 or any species of formula  $[Ni_x(GC-OMe)_x(S'Bu)]^-$  are observed via ESI-MS<sup>-</sup>. These results suggest a dynamic situation involving potential Sbridging interactions, loss of monodentate thiolate, and possible aquation/solvation for 2-5 in H<sub>2</sub>O and other protic media. It is not too surprising that an equilibrium exists with our peptide ligands as a nonapeptide Ni-SOD maquette analogue has been shown to exist in equilibrium with a 2:1 Ni/peptide and 1:1 Ni/peptide species in solution via UV-vis titrations. <sup>30</sup> However, ESI-MS measurements reveal a 1:2 Ni/peptide ratio with considerable amount of free peptide. These seemingly contradictory results clearly establish that, in the absence of the Ni-SOD protein quaternary structure, the probability of multiple Ni-L (where L is a generic representation of any peptido-N/thiolato-S ligand) species is high at least in water. To support this proposal, the <sup>1</sup>H NMR spectra of as isolated 2–5 in CD<sub>3</sub>CN display no evidence of such behavior and provide clean diamagnetic spectra consistent with their [Ni(GC-OMe)(SR)] formulation (supporting information). Thus, the as-isolated Ni(II) monomeric complexes remain fully intact in polar aprotic solvents, which further support the notion that the equilibrium is promoted by interaction with solvent protons.

#### Electronic absorption spectroscopy

The UV-vis spectra of 2-5 in DMF or pH 7.5 buffer (PIPES) at 298 K display two predominant features in the visible region (~ 470 and 550 nm) consistent with the red-violet color of these solutions and similar in nature to Ni-SOD<sub>red</sub>. <sup>22</sup> In DMF, the most intense visible band is broad and ranges from 463 nm ( $\epsilon$ : 350 M<sup>-1</sup> cm<sup>-1</sup>) for 5 to 484 nm ( $\epsilon$ : 450 M<sup>-1</sup> cm<sup>-1</sup>) for **3** (Figure 2, Table 1); similar visible transitions are observed in Ni-SOD<sub>red</sub> at 450 nm ( $\epsilon$ : 480 M<sup>-1</sup> cm<sup>-1</sup>)<sup>22</sup> and other square-planar Ni(II)N<sub>2</sub>S<sub>2</sub> complexes.<sup>34–35,62–68</sup> These absorptions are proposed to be ligand-field (d-to-d) transitions containing a minor charge-transfer (CT) contribution.<sup>22</sup> A second less intense ligand-field transition appears as a shoulder between 545 nm ( $\epsilon$ : 160 M<sup>-1</sup> cm<sup>-1</sup>) for **5** and 570 nm (230 M<sup>-1</sup> cm<sup>-1</sup>) for **3** and mirrors a similar feature in Ni-SOD<sub>red</sub> at 543 nm (e: 150 M<sup>-1</sup> cm<sup>-1</sup>). The high energy band at 361 nm ( $\epsilon$ : 880 M<sup>-1</sup> cm<sup>-1</sup>) in Ni-SOD<sub>red</sub> is also observed in 3 ( $\lambda_{max}$ : 358 nm;  $\epsilon$ : 1,410  $M^{-1}$  cm<sup>-1</sup>) and 5 ( $\lambda_{max}$ : 358 nm;  $\epsilon$ : 1,230  $M^{-1}$  cm<sup>-1</sup>) further underscoring the electronic structural similarities between our models and the enzyme (Figure S1). The same high energy feature is difficult to elucidate in 2 and 4 due to the presence of an overwhelming transition in the UV, presumably  $\pi$ - $\pi$ \* in nature. UV-vis spectra of 2, 4 and 5 in buffer do not differ much from those in DMF (Figure 2, Table 1) suggesting that the various Ni(II) species present retain GC-OMe<sup>2-</sup> ligation. For example,  $\lambda_{max}$ : 471 nm ( $\epsilon$ : 420 M<sup>-1</sup> cm<sup>-1</sup>) for **2** and 458 nm ( $\epsilon$ : 560 M<sup>-1</sup> cm<sup>-1</sup>; 280 M<sup>-1</sup> cm<sup>-1</sup>/Ni) for **1**. Similarly, the less intense feature appears at 545 nm ( $\epsilon$ : 140 M<sup>-1</sup> cm<sup>-1</sup>) for **5** and 560 nm ( $\epsilon$ : 240 M<sup>-1</sup> cm<sup>-1</sup>) for **2** is somewhat less pronounced than in the DMF samples. Higher energy transitions at  $\lambda_{max}$  ~ 338 nm are also present for 2 and 5 (Figure S2). Interestingly, dissolution of 3 in buffer provides a spectral profile identical to dimer 1, suggestive of protonation and loss of the more basic <sup>t</sup>BuS<sup>-</sup> ligand.

Since the aqueous electronic absorption spectra of as-isolated **2**, **4**–**5** represent an equilibrium mixture of Ni(II) species we also recorded their spectra in the presence of excess thiolate to generate one monomeric species (see NMR discussion above). When one mol-equiv of KSC<sub>6</sub>H<sub>4</sub>-*p*-Cl, KSC<sub>6</sub>H<sub>4</sub>-*p*-OMe, and HSNAc are added to as-isolated buffered solutions of **2**, **4**, **5**, respectively, only subtle changes in the visible region of the UV-vis spectra resulted. For example, the lowest-energy ligand-field shoulder between 545–560 nm becomes more pronounced for all complexes (Figures S30–32). As discussed above, **3** forms dimer **1** when dissolved in buffer. Even addition of up to five mol-equiv of KS'Bu to as-isolated **3** affords no changes in the UV-vis. Collectively, these results suggest that the

Ni(II) species present upon dissolution of as-isolated **2**, **4**–**5** in buffer are electronically similar to the formally monomeric species that form in the presence of excess RS<sup>-</sup>.

Taken together, the similarities between the electronic absorption spectra of 1–5 and Ni-SOD<sub>red</sub> suggest that our models successfully reproduce the electronic environment of the NiN<sub>2</sub>S<sub>2</sub> unit in the enzyme active site (Table 1). One interesting point to note when comparing spectra obtained in DMF and buffer is that the ligand-field transitions of 2 and 4 blue-shift ~ 10 nm in buffer, however, complex 5 does not shift at all. An attractive explanation is that the peptide-NH of the SNAc<sup>-</sup> ligand forms an intramolecular H-bond with the thiolato-S ligands in DMF in a manner approximating aqueous H-bonding interactions.<sup>37</sup> The observation that  $\delta_{NH}$  shifts by > 1 ppm downfield in the <sup>1</sup>H NMR (8.62 ppm in CD<sub>3</sub>CN) of the tethered peptide of NAc-S<sup>-</sup> in 5 (supporting information) compared to  $\delta_{NH}$  of free SNAc (7.43 ppm) suggest that intramolecular H-bonding interactions are present. Prior experimental and theoretical investigations pertaining to NAc-S<sup>-</sup> bound to the Ni(nmp) synthon also corroborate this notion.<sup>37</sup> Furthermore, the spontaneous loss of the 'BuS<sup>-</sup> ligand from 3 in buffer provide supporting evidence for the interaction of the coordinated thiolates with solvent protons in these systems.

#### Electrochemistry

Cyclic voltammetry (CV) measurements in DMF show irreversible oxidation ( $E_{ox}$ ) events for 2-5 (Figure 3, Table 1). Irreversible CVs have been a hallmark of Ni(II)-N<sub>2</sub>S<sub>2</sub> SOD models<sup>34–35,37–38</sup> and indicate an overall change in the coordination environment after oxidation, most likely a result of a thiolate-disulfide conversion, which is prevented in the enzyme. Comparison of the potentials demonstrated patterns which can be roughly correlated to the donor strength of the monodentate RS $^-$  ligand. For example,  $E_{\rm ox}$  for the reported complexes increase (more difficult to oxidize) in the following order: 3 (0.080 V vs. Ag/AgCl) < 4 (0.170 V) < 2 (0.220 V) < 5 (0.310 V). This observation corresponds well with the trend established using the Ni(nmp) synthon showing the redox potentials of  $[Ni(N_2S)(SR)]^-$  complexes increase as the donor strength of the exogenous RS<sup>-</sup> decreases when separately analyzing complexes featuring RS<sup>-</sup> of aryl and alkyl nature.<sup>37</sup> As observed in the UV-vis studies, complexes featuring alkyl RS<sup>-</sup> donors tend to be more sensitive to electronic perturbations such as intramolecular H-bonding and solvent environment. In pH 7.4 buffer (phosphate)  $E_{ox}$  follows: 2 (0.285 V vs. Ag/AgCl) < 4 (0.315 V) < 5 (0.550 V) (Figure 3, Table 1). Comparing 2 and 4, it is evident that the more positive redox event belongs to the complex with the more strongly donating RS-. Amongst the alkyl RS- no comparison is available due to the spontaneous dissociation of 'BuS' from 3 in buffer (1 shows no redox waves up to +1.000 V). In fact, a second  $E_{ox}$  is observed in the CV of 4 at 0.480 V which was found to match that of KSC<sub>6</sub>H<sub>4</sub>-p-OMe dissolved in the same buffer and suggests that facile RS<sup>-</sup> dissociation observed in 3 occurs in 4 as well albeit to a lesser magnitude. The RS- protonation/dissociation observed in buffer points towards strong interactions between RS<sup>-</sup> and solvent protons. Manifestation of such an interaction is expected to increase with increasing RS- basicity, and serves to rationalize the reverse trend in  $E_{\rm ox}$  of 2 and 4 as well as the observed dissociation of the more basic thiolates. In accordance with this hypothesis, shifts of 0.065, 0.145 and 0.220 V to more positive potentials is observed for 2, 4 and 5, respectively, when comparing the potentials obtained in buffer to those in DMF; a trend which also correlates to relative RS<sup>-</sup> basicity.

The  $E_{\rm ox}$  values for 2–5 arise at potentials which are distinct from those obtained for free ligand and the K<sup>+</sup> salts of their respective RS<sup>-</sup> ligands in both DMF and buffer, supporting the notion that the redox-active species present are indeed the Ni(II) complexes and not dissociated RS<sup>-</sup>. It should also be noted that addition of one mol-equiv of the appropriate RS<sup>-</sup> or HSR ligand to solutions of the as-isolated complexes provided no change in  $E_{\rm ox}$ ,

consistent with the aforementioned observation (UV-vis, above) that the species present upon dissolution of as-isolated 2, 4 and 5 in aqueous buffer are of an electronically similar disposition to the corresponding discreet monomeric species. The recorded  $E_{ox}$  values also fall between the 0.04-1.09 V (vs. Ag/AgCl) potential window defined by the two SOD half reactions, <sup>69</sup> and imply that these complexes are thermodynamically poised for at least one turnover. However, the irreversible nature of the CV demonstrate that the Ni(III) state obtained during catalysis in the enzyme is not stabilized in these models. Not surprisingly, no Ni-SOD peptide maquette or small molecule analogue has ever been isolated in the corresponding Ni(III) states and attempts at chemical oxidation result in complex degradation, most likely via disulfide formation.<sup>28</sup> In fact, disulfide formation of the coordinated monodentate thiolate in 2, 4 and 5 appear to be responsible for the reported  $E_{\rm ox}$ . Bulk oxidation of 2 with one mol-equiv of a ferrocenium salt afforded 1 and the disulfide of para-chlorobenzene thiol in quantitative yield. Accordingly, these complexes provide no protection against superoxide reduction of p-nitroblue tetrazolium chloride (NBT) to its ring-open formazan form in the presence of 25 mol-equiv of KO<sub>2</sub>.<sup>70</sup> It should be noted that the addition of up to 10 mol-equiv of an exogenous N-donor such as imidazole imparted no SOD activity or electrochemical reversibility as measured by CV.

## X-ray absorption spectroscopy (XAS)

Although single crystals of the Ni-peptide complexes were not obtained, we were able to get limited structural information on these systems through Ni K-edge X-ray absorption spectroscopy (XAS). The XAS acquired for complexes 2 and 5 reveal Ni(II) systems with an approximately square-planar coordination geometry about the metal center. The XANES area of the spectrum confirm this assignment as each complex displays an intense pre-edge peak corresponding to a  $1s \rightarrow 4p_z$  transition at ~ 8336 eV (see Figure 4 and Table 2), which is characteristic of Ni(II) in  $D_{4h}$  (square-planar) symmetry. <sup>71</sup> For comparison, XAS were acquired on members of the crystallographically-characterized (Et<sub>4</sub>N)[Ni(nmp)(SR)] family of complexes which also afford similar edge features to 2 and 5 as further confirmation of the square-planar nature of the systems reported here. The EXAFS region of 2 and 5 are best-fit with two non-equivalent Ni-N scatterers at 1.83(3) Å and 1.96(3) Å, which we assign as the Ni-N<sub>peptide</sub> and Ni-N<sub>amine</sub>, respectively based on EXAFS of the Ni(nmp) complexes (see Table 2 and the supporting information). To complete the NiN<sub>2</sub>S<sub>2</sub> coordination sphere, two Ni-S scatterers are also observed at an average distance of 2.16(2) Å. These distances compare well with other Ni-N<sub>2</sub>S<sub>2</sub> SOD models, <sup>34–35,37–38</sup> peptide maquettes, <sup>28</sup> and the enzyme itself. <sup>17–19</sup> The XAS thus complement the UV-vis, ESI-MS, and <sup>1</sup>H NMR studies and reveal that the reported Ni(II)-peptide complexes are excellent structural and spectroscopic analogues of Ni-SOD<sub>red</sub>.

#### Relationship to Ni-SOD

Ligand-substitution in square-planar  $d^8$  complexes generally follow an associative or interchange pathway where a five-coordinate (5C) trigonal bipyramidal intermediate is invoked in the transition state. In the present systems, one may assume a 5C intermediate is traversed (and may be stabilized) during spontaneous RS<sup>-</sup> dissociation in aqueous buffer. The formation of a higher coordination number species would explain the broadness in the <sup>1</sup>H NMR spectra due to potential Ni(II) S = 1 solvated derivatives that form once the monodentate thiolate is lost. Recent mutagenesis studies by Maroney and Brunold on Ni-SOD at Cys2, Cys6 and Cys2/Cys6 (double mutant) have shown that even the absence of one cysteine thiolate promotes high-spin (S = 1) aquated Ni(II) complexes at the Ni-SOD active site *with no evidence of the remaining Ni-SCys bond in the single mutants*. This finding in combination with the results reported here suggests more than redox-modulation/H-storage roles for cysteine in Ni-SOD. We propose that both Cys6 and Cys2 ligands in Ni-SOD are crucial for proper active site assembly and stabilization of the low-spin square-

planar Ni(II) state. This explanation is similar to the advocated H-bond directionality and positioning that Val8 and Glu17 impart on His1 especially towards formation of the Ni(III)-NHis bond in Ni-SOD<sub>ox</sub>. Perhaps this hypothesis also explains the various Ni/peptide stoichiometries observed in other Ni-SOD maquettes<sup>30</sup> as well as the chiral inversion seen in the Ni(NCC) tripeptide complex<sup>33</sup> over time. While the hexameric quaternary structure of Ni-SOD likely precludes Cys6 dissociation, cysteinate protonation may be sufficient to trigger weak binding of the His1 imidazole and further destabilization of the Ni(II) center, despite the futility of the pathway with regards to ligand exchange. The promiscuous nature of these SOD models in buffer underscores the importance of the immediate environment surrounding the active site and points to a role for secondary and tertiary-sphere residues in the overall structure and in preserving the integrity of the mononuclear assembly. Accordingly, the six Ni centers of the Ni-SOD hexamer comprise the vertices of an octahedron with a large interior cavity and are separated by a minimum distance of 23 Å. 17-18 It should be noted that Ni-S complexes featuring monodentate thiolate ligands are notorious for oligomerization in protic media.<sup>54</sup> In fact, to the best of our knowledge, there remains a paucity of literature precedence for monomeric, heteroleptic Ni-SR complexes featuring monodentate thiolates<sup>72</sup> outside of our research and none pertaining to the characterization of such species in protic solvent.

## **Conclusions**

The above work on the metallopeptide derived complexes 1–5 provide the first aqueous studies pertaining to isolable, small molecule Ni-SOD biomimetics. The dimeric complex 1 serves as a suitable metallosynthon to generate several unique Ni(II)-N<sub>2</sub>S<sub>2</sub> complexes with one variable basal plane coordination site. The electronic absorption spectra of the resulting monomers 2-5 in both DMF and pH 7.5 buffer compare well with that obtained for Ni-SOD<sub>red</sub> and suggest that our [Ni(GC-OMe)(SR)]<sup>-</sup> models of similar electronic structure to Ni-SOD<sub>red</sub>. CV measurements in DMF and buffer display irreversible oxidation events within the potential window defined by the SOD half reactions. The CV data suggests that while our mimics are electrochemically capable of promoting SOD chemistry, the Ni(III) state is not accessible, which is crucial for catalysis. Apparently the N<sub>2</sub>S<sub>2</sub> planar ligand lacks electrochemical stabilization needed to support a competent SOD mimetic. The failure of our models to provide protection of NBT from superoxide reduction corroborates this notion. This lack of electrochemical reversibility and SOD activity may be attributed to the lack of an axial N-donor or the absence of the protective shell of the protein to stabilize a higher coordinate structure. The <sup>1</sup>H NMR spectra of as isolated 2–5 in D<sub>2</sub>O provide broad, ill-resolved signals which may correspond to a variety of species present, perhaps in exchange with one another or with solvent. However, addition of one mol-equiv of the appropriate thiolate ligand did afford spectra with well-resolved splitting patterns consistent with a monomeric diamagnetic species. Dissolution of as-isolated 2-5 in CD<sub>3</sub>CN afforded neat, readily discernable <sup>1</sup>H NMR spectra consistent with discrete species, suggesting that further speciation is assisted via interaction with protic media. The NMR data in D<sub>2</sub>O coupled with ESI-MS analysis revealed various species of general formula, [Ni<sub>1-4</sub>(GC-OMe)<sub>1-4</sub>(SR)]<sup>-</sup>, and suggest that the active site fragment of Ni-SOD may be a rather dynamic species with a propensity to oligomerize outside of the protein matrix. Thus, the surrounding environment may be crucial to maintaining coordinative integrity. At present, we are undertaking studies pertaining to the role played by the axial imidazole-N donor and exploring ligand modifications with the aim of achieving electrochemical reversibility and ultimately SOD activity.

# **Supplementary Material**

Refer to Web version on PubMed Central for supplementary material.

## **Acknowledgments**

T.C.H. acknowledges support from the National Science Foundation (CAREER grant: CHE-0953102).

#### References

 Beyer W, Imlay J, Fridovich I. Prog. Nucleic Acid Res. Mol. Biol. 1991; 40:221. [PubMed: 1851570]

- Maritim AC, Sanders RA, Watkins JB. J. Biochem. Mol. Toxicol. 2003; 17:24. [PubMed: 12616644]
- 3. Valentine JS, Wertz DL, Lyons TJ, Liou L-L, Goto JJ, Gralla EB. Curr. Opin. Chem. Biol. 1998; 2:253. [PubMed: 9667937]
- Kumar B, Koul S, Khandrika L, Meacham RB, Koul HK. Cancer Res. 2008; 68:1777. [PubMed: 18339858]
- 5. Ishikawa K, Takenaga K, Akimoto M, Koshikawa N, Yamaguchi A, Imanishi H, Nakada K, Honma Y, Hayashi J-I. Science. 2008; 320:661. [PubMed: 18388260]
- Fortunato G, Pastinese A, Intrieri M, Lofrano MM, Gaeta G, Censi MB, Boccalatte A, Salvatore F, Sacchetti L. Clin. Biochem. 1997; 30:569. [PubMed: 9399027]
- 7. Kocatürk PA, Akbostanci MC, Tan F, Kavan GO. Pathophysiology. 2000; 7:63. [PubMed: 10825687]
- 8. Riley DP. Chem. Rev. 1999; 99:2573. [PubMed: 11749493]
- De Leo ME, Borrello S, Passantino M, Palazzotti B, Mordente A, Daniele A, Filippini V, Galeotti T, Masullo C. Neurosci. Lett. 1998; 250:173. [PubMed: 9708860]
- 10. Auchére F, Rusnak FJ. Biol. Inorg. Chem. 2002; 7:664.
- 11. Tierney DL, Fee JA, Ludwig ML, Penner-Hahn JE. Biochemistry. 1995; 34:1661. [PubMed: 7849025]
- 12. Miller A-F. Curr. Opin. Chem. Biol. 2004; 8:162. [PubMed: 15062777]
- 13. Borgstahl GEO, Parge HE, Hickey MJ, Beyer WF, Hallewell RA, Tainer JA. Cell. 1992; 71:107. [PubMed: 1394426]
- Tainer JA, Getzoff ED, Richardson JS, Richardson DC. Nature. 1983; 306:284. [PubMed: 6316150]
- 15. Youn H-D, Youn H, Lee J-W, Yim Y-I, Lee JK, Hah YC, Kang S-O. Arch. Biochem. Biophys. 1996; 334:341. [PubMed: 8900409]
- 16. Youn H-D, Kim E-J, Roe J-H, Hah YC, Kang S-O. Biochem. J. 1996; 318:889. [PubMed: 8836134]
- 17. Barondeau DP, Kassmann CJ, Bruns CK, Tainer JA, Getzoff ED. Biochemistry. 2004; 43:8038. [PubMed: 15209499]
- Wuerges J, Lee J-W, Yim Y-I, Yim H-S, Kang S-O, Carugo KD. Proc. Natl. Acad. Sci. U.S.A. 2004; 101:8569. [PubMed: 15173586]
- Choudhury SB, Lee JW, Davidson G, Yim YI, Bose K, Sharma ML, Kang SO, Cabelli DE, Maroney MJ. Biochemistry. 1999; 38:3744. [PubMed: 10090763]
- Bryngelson PA, Arobo SE, Pinkham JL, Cabelli DE, Maroney MJ. J. Am. Chem. Soc. 2004;
   126:460. [PubMed: 14719931]
- 21. Ryan KC, Johnson OE, Cabelli DE, Brunold TC, Maroney MJ. J. Biol. Inorg. Chem. 2010; 15:795. [PubMed: 20333421]
- Fiedler AT, Bryngelson PA, Maroney MJ, Brunold TC. J. Am. Chem. Soc. 2005; 127:5449.
   [PubMed: 15826182]
- 23. Johnson OE, Ryan KC, Maroney MJ, Brunold TC. J. Biol. Inorg. Chem. 2010; 15:777. [PubMed: 20333422]
- 24. Herbst RW, Guce A, Bryngelson PA, Higgins KA, Ryan KC, Cabelli DE, Garman SC, Maroney MJ. Biochemistry. 2009; 48:3354. [PubMed: 19183068]
- 25. Szilagyi RK, Bryngelson PA, Maroney MJ, Hedman B, Hodgson KO, Solomon EI. J. Am. Chem. Soc. 2004; 126:3018. [PubMed: 15012109]

- 26. Neupane KP, Shearer J. Inorg. Chem. 2006; 45:10552. [PubMed: 17173410]
- 27. Shearer J, Neupane KP, Callan PE. Inorg. Chem. 2009; 48:10560. [PubMed: 19894770]
- 28. Shearer J, Long LM. Inorg. Chem. 2006; 45:2358. [PubMed: 16529443]
- 29. Neupane KP, Gearty K, Francis A, Shearer JJ. Am. Chem. Soc. 2007; 129:14605.
- 30. Tietze D, Breitzke H, Imhof D, Kothe E, Weston J, Buntkowsky G. Chem. Eur. J. 2009; 15:517. [PubMed: 19016282]
- 31. Schmidt M, Zahn S, Carella M, Ohlenschläger O, Görlach M, Kothe E, Weston J. ChemBioChem. 2008; 9:2135. [PubMed: 18690655]
- 32. Krause ME, Glass AM, Jackson TA, Laurence JS. Inorg. Chem. 2010; 49:362. [PubMed: 20000358]
- 33. Krause ME, Glass AM, Jackson TA, Laurence JS. Inorganic Chemistry. 2011; 50:2479. [PubMed: 21280586]
- 34. Mathrubootham V, Thomas J, Staples R, McCraken J, Shearer J, Hegg EL. Inorg. Chem. 2010; 49:5393. [PubMed: 20507077]
- 35. Shearer J, Zhao N. Inorg. Chem. 2006; 45:9637. [PubMed: 17112256]
- 36. Shearer J, Dehestani A, Abanda F. Inorg. Chem. 2008; 47:2649. [PubMed: 18330983]
- 37. Gale EM, Narendrapurapu BS, Simmonett AC, Schaefer HF, Harrop TC. Inorg. Chem. 2010; 49:7080. [PubMed: 20575514]
- 38. Gale EM, Patra AK, Harrop TC. Inorg. Chem. 2009; 48:5620. [PubMed: 20507097]
- 39. Ma H, Chattopadhyay S, Petersen JL, Jensen MP. Inorg. Chem. 2008; 47:7966. [PubMed: 18710223]
- 40. Ma H, Wang G, Yee GT, Petersen JL, Jensen MP. Inorg. Chim. Acta. 2009; 362:4563.
- 41. Pelmenschikov V, Siegbahn PEM. J. Am. Chem. Soc. 2006; 128:7466. [PubMed: 16756300]
- 42. Mullins CS, Grapperhaus CA, Kozlowski PM. J. Biol. Inorg. Chem. 2006; 11:617. [PubMed: 16724228]
- 43. Prabhakar R, Morokuma K, Musaev DG. J. Comput. Chem. 2006; 27:1438. [PubMed: 16804959]
- 44. Volbeda A, Charon MH, Piras C, Hatchikian EC, Frey M, Fontecilla-Camps JC. Nature. 1995; 373:580. [PubMed: 7854413]
- 45. Ermler U, Grabarse W, Shima S, Goubeaud M, Thauer RK. Science. 1997; 278:1457. [PubMed: 9367957]
- 46. Dobbek H, Svetlitchnyi V, Gremer L, Huber R, Meyer O. Science. 2001; 293:1281. [PubMed: 11509720]
- 47. Doukov TI, Iverson TM, Seravalli J, Ragsdale SW, Drennan CL. Science. 2002; 298:567. [PubMed: 12386327]
- 48. Darnault C, Volbeda A, Kim EJ, Legrand P, Vernede X, Lindahl PA, Fontecilla-Camps JC. Nat. Struct. Biol. 2003; 10:271. [PubMed: 12627225]
- 49. Krüger H-J, Peng G, Holm RH. Inorg. Chem. 1991; 30:734.
- 50. Fox S, Wang Y, Silver A, Millar M. J. Am. Chem. Soc. 1990; 112:3218.
- 51. Pavlov M, Siegbahn PEM, Blomberg MRA, Crabtree RH. J. Am. Chem. Soc. 1998; 120:548.
- 52. Niu SQ, Thomson LM, Hall MB. J. Am. Chem. Soc. 1999; 121:4000.
- 53. Amara P, Volbeda A, Fontecilla-Camps JC, Field MJ. J. Am. Chem. Soc. 1999; 121:4468.
- 54. Rosenfield SG, Armstrong WH, Mascharak PK. Inorg. Chem. 1986; 25:3014.
- 55. O'Reilly JE. Biochim. Biophys. Acta. 1973; 292:509. [PubMed: 4705442]
- 56. Scott, RA. Physical methods in Bioinorganic Chemistry: Spectroscopy and Magnetism. Que, L., Jr, editor. Sausalito, CA: University Science Books; 2000. p. 465
- 57. Gennari M, Orio M, Pécaut J, Neese F, Collomb MN, Duboc C. Inorg. Chem. 2010; 49:6399. [PubMed: 20553029]
- 58. Jenkins RM, Singleton ML, Almaraz E, Reibenspies JH, Darensbourg MY. Inorg. Chem. 2009; 48:7280. [PubMed: 19572492]
- Jenkins RM, Singleton ML, Leamer LA, Reibenspies JH, Darensbourg MY. Inorg. Chem. 2010;
   49:5503. [PubMed: 20507173]

- 60. Baidya N, Olmstead MM, Mascharak PK. Inorg. Chem. 1991; 30:3967.
- 61. Silverstein, RM.; Webster, FX.; Kiemle, DJ. Spectrometric Identification of Organic Compounds. Hoboken, NJ: Wiley; 2005.
- 62. Mills DK, Reibenspies JH, Darensbourg MY. Inorg. Chem. 1990; 29:4364.
- 63. Smee JJ, Miller ML, Grapperhaus CA, Reibenspies JH, Darensbourg MY. Inorg. Chem. 2001; 40:3601. [PubMed: 11421712]
- 64. Farmer PJ, Reibenspies JH, Lindahl PA, Darensbourg MY. J. Am. Chem. Soc. 1993; 115:4665.
- 65. Grapperhaus CA, Maguire MJ, Tuntulani T, Darensbourg MY. Inorg. Chem. 1997; 36:1860. [PubMed: 11669791]
- 66. Colpas GJ, Kumar M, Day RO, Maroney MJ. Inorg. Chem. 1990; 29:4779.
- 67. Hanss J, Krüger H-J. Angew. Chem. Int. Ed. 1998; 37:360.
- Maroney MJ, Choudhury SB, Bryngelson PA, Mirza SA, Sherrod MJ. Inorg. Chem. 1996;
   35:1073. [PubMed: 11666287]
- 69. Sawyer DT, Valentine JS. Acc. Chem. Res. 1981; 14:393.
- Tabbì G, Driessen WL, Reedijk J, Bonomo RP, Veldman N, Spek AL. Inorg. Chem. 1997;
   36:1168. [PubMed: 11669684]
- Gu Z, Dong J, Allan CB, Choudhury SB, Franco R, Moura JJG, Moura I, LeGall J, Przybyla AE, Roseboom W, Albracht SPJ, Axley MJ, Scott RA, Maroney MJ. Journal of the American Chemical Society. 1996; 118:11155.
- 72. Huang D, Deng L, Sun J, Holm RH. Inorg. Chem. 2009; 48:6159. [PubMed: 19459662]

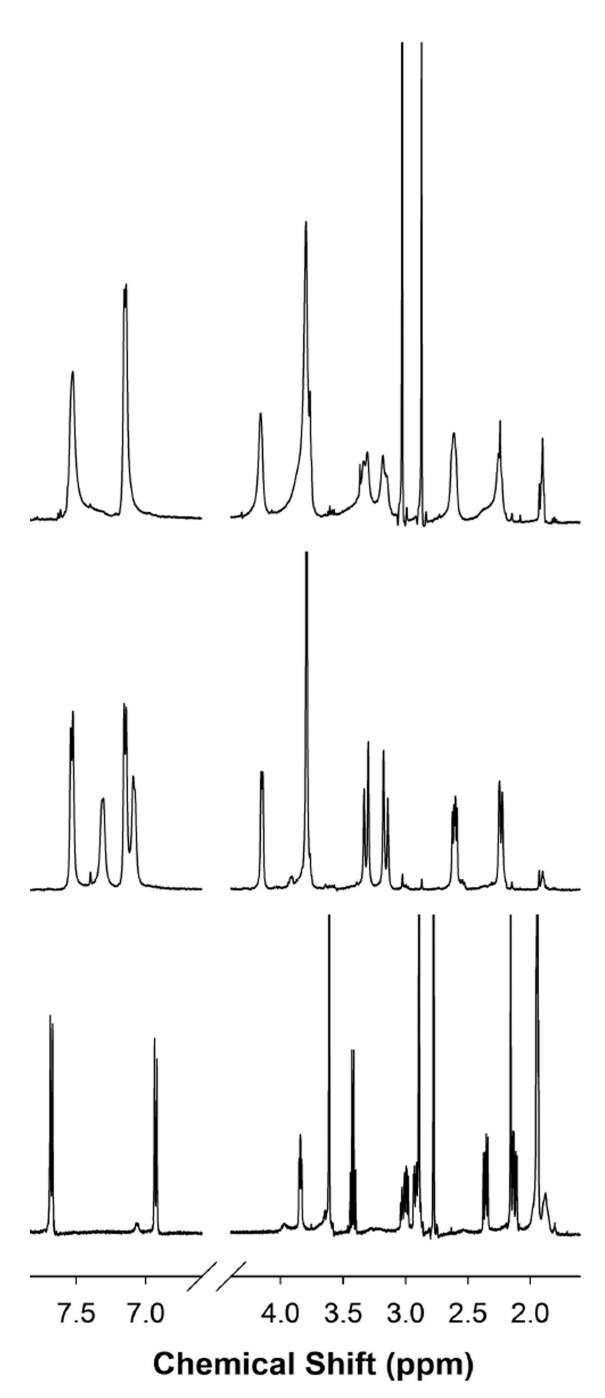


**Figure 1.**<sup>1</sup>H NMR spectrum of **2** recorded under different conditions at 298 K. (Top): As-isolated **2** in D<sub>2</sub>O (signals at 3.01 and 2.85 ppm correspond to DMF associated with isolated product). (Middle): Complex **2** in D<sub>2</sub>O after the addition of one mol-equiv of KSC<sub>6</sub>H<sub>4</sub>-*p*-Cl (doublets at 7.41 and 7.19 (at right) correspond to free non-coordinated KSC<sub>6</sub>H<sub>4</sub>-*p*-Cl). (Bottom): Asisolated **2** in CD<sub>3</sub>CN (signal at 3.42 corresponds to Et<sub>2</sub>O present in the sample; 2.89 and 2.77 correspond to DMF associated with isolated product; 1.94 arises from residual protio solvent).

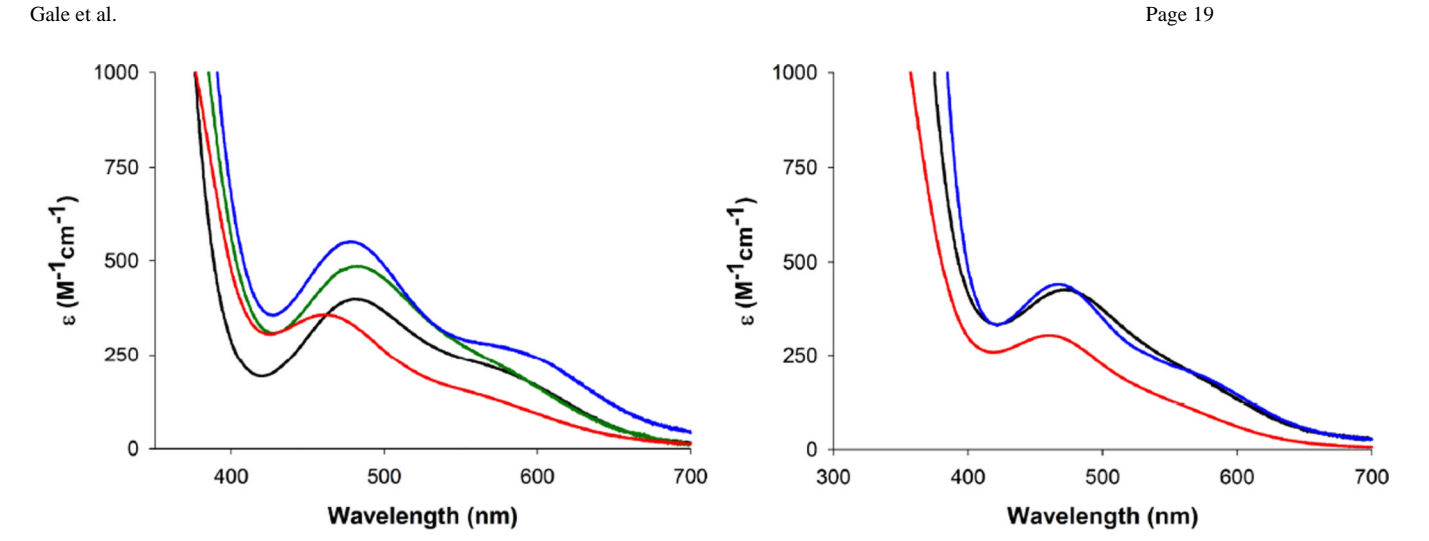


Figure 2. Electronic absorption spectra for 2 (black), 3 (green), 4 (blue) and 5 (red) in DMF (left) and of 2, 4 and 5 in pH 7.5 PIPES buffer (right) recorded at 298 K.

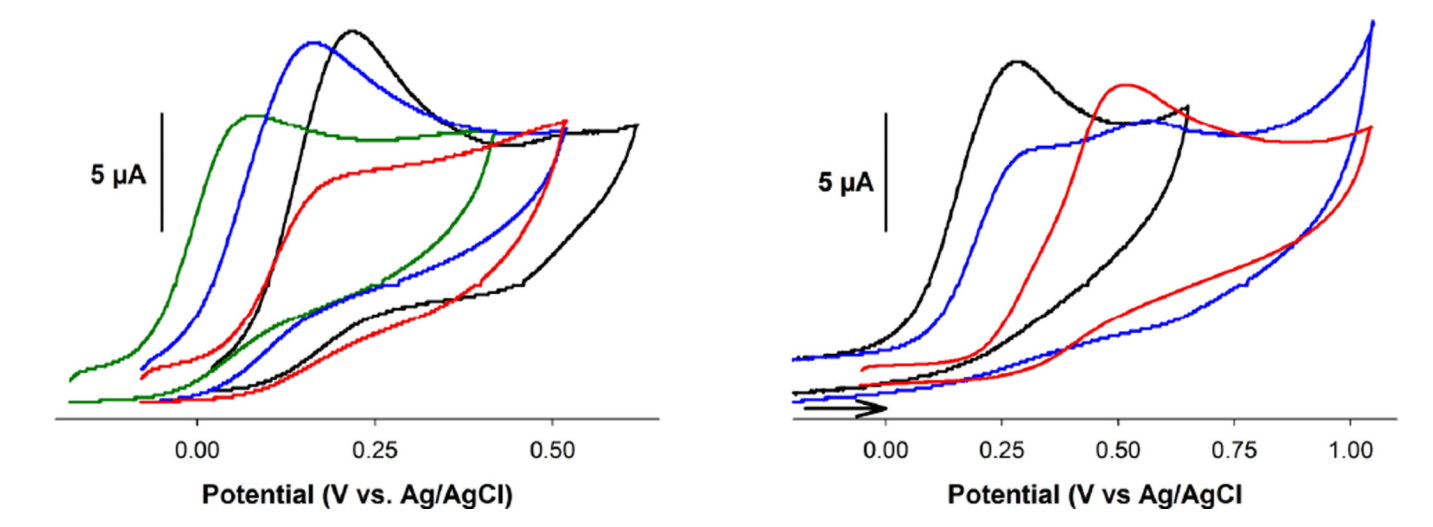


Figure 3. Cyclic voltammograms (CVs) of 5 mM solutions of 2 (black), 3 (green), 4 (blue) and 5 (red) (vs.  $Ag/Ag^+$  in DMF (0.01 M  $AgNO_3/0.1$  M  $^nBu_4NPF_6$  in MeCN), 0.1 M  $^nBu_4NPF_6$  supporting electrolyte, glassy carbon working electrode, scan rate: 100 mV/s, RT) (left). CVs of 5 mM solutions of 2, 4 and 5 (vs. Ag/AgCl in pH 7.4 phosphate buffer, 0.5 M KNO $_3$  supporting electrolyte, glassy carbon working electrode, scan rate: 100 mV/s, RT) (right). Arrow indicates direction of scan.

Gale et al.

0.0

0

2

3

R' (Å)

2.0 2.0 Normalized Intensity Normalized Intensity 0.0 0.0 8300 8320 8340 8360 8380 8400 8300 8320 8340 8360 8380 8400 Energy (eV) Energy (eV) 10 10  $k^3 \chi(k)$ -5 -5 -10 2 6 8 10 12 6 10 12 2 8  $k (\mathring{A}^{-1})$  $k (Å^{-1})$ 2.5 2.5 2.0 2.0 FT Magnitude 0.5 0.5 FT Magnitude 0.0 5

Page 21

Figure 4. Ni K-edge X-ray absorption data for K[Ni(GC-OMe)(S-p-C<sub>6</sub>H<sub>4</sub>Cl)] (2) (left) and K[Ni(GC-OMe)(S-NAc)] (5) (right). *Top*: Edge spectra displaying Ni (1s  $\rightarrow$  4p<sub>z</sub>) transition consistent with square-planar Ni(II). *Middle*: FF  $k^3$  EXAFS data. *Bottom*: FT  $k^3$  EXAFS data. Experimental data are in black with simulations in red.

6

5

0.0

0

3

R' (Å)

6

5

$$\mathbf{M}^{\mathbf{ox}} + \mathbf{O}_2^{\bullet -} \longrightarrow \mathbf{M}^{\mathbf{red}} + \mathbf{O}_2 \tag{1}$$

$$M^{red} + O_2^{\bullet -} + 2 H^+ \longrightarrow M^{ox} + H_2O_2$$
 (2)

Scheme 1.

Chemistry catalyzed by SOD split into half-reactions.

$$\frac{\text{BOC-Gly-OSu}}{\text{CH}_2\text{Cl}_2,\,\text{RT}} \text{ MeO} \xrightarrow{\text{NH}} \text{NH} \xrightarrow{\text{N}} \text{CF}_3\text{CO}_2\text{H}$$

$$\frac{\text{Et}_3\text{SiH}}{\text{TFA/CH}_2\text{Cl}_2\,\,(1:1),\,\text{RT}} \text{ MeO} \xrightarrow{\text{N}} \text{NH} \xrightarrow{\text{N}} \text{NH}_2 \bullet \text{CF}_3\text{CO}_2\text{H}$$

$$\frac{\text{SH}}{\text{SH}} \xrightarrow{\text{CC-OMeH}_2 \bullet \text{TFA}} \text{ GC-OMeH}_2 \bullet \text{TFA}$$

**Scheme 1.** Synthesis of GC-OMeH<sub>2</sub>.

**Scheme 2.** Synthesis of Ni(II) Complexes **2–5**.

R:  $\{(2), (3), (4), (5), (5), (6), (10),$ 

(Top): Active Site of Ni-SOD<sub>ox</sub> (left), Ni-SOD<sub>red</sub> (middle), and Ni-SOD<sub>red</sub> analogues described in the present work, [Ni(GC-OMe)(SR)]<sup>-</sup> (right). (Bottom): R groups used in this study.

Table 1

Spectroscopic (UV-vis) and electrochemical (CV) properties of 2-5 in the listed solvents in comparison to Ni-peptide magnettes and Ni-SOD<sub>red</sub>.

Gale et al.

Ag/AgCl) in buffer	0.285 this work	N/Ad this work	0.315 this work	0.550 this work	0.520 29	0.487 22.24
Ag/Ag/CI) $Ag/Ag/CIin DMF in buffer$	0.220	0.080	0.170	0.310	N/A	N/A
λ <sub>max</sub> , nm (e, M <sup>-1</sup> cm <sup>-1</sup> ) in buffer	471 (430) 560 (240)	$ ho { m V/N}$	467 (420) 550 (230)	463 (300) 545 (140)	457 (345) 548 (130)	450 (480) 543 (150)
$\lambda_{ ext{max}}$ , nm (e, M <sup>-1</sup> cm <sup>-1</sup> ) in DMF	481 (390) 560 (230)	484 (450) 570 (240)	480 (510) 565 (250)	463 (350) 545 (160)	N/A	N/A
Complex	$2^a$	3a	<b>4</b> a	5a	$Ni(SOD^{M1})^b$	$ ext{Ni-SOD}_{ ext{red}}^{c}$

<sup>a</sup>All spectra and CV (E<sub>OX</sub> reported) recorded at 298 K; Spectra recorded in pH 7.5 PIPES buffer, CV recorded in pH 7.4 phosphate buffer.

 $^{b}M1 = H_2N$ -HCDLPCG-OH;  $^{29}$  spectra and CV recorded (quasi-reversible  $E_{1/2}$  reported) at RT in pH 7.4 NEM buffer (0.1 M NaClO4 electrolyte for CV).  $^{29}$ 

<sup>C</sup>Redox titration ( $E_{1/2}$  originally referenced versus NHE = 0.290 V)<sup>24</sup> recorded at RT in pH 7.5 phosphate buffer.

 $d_{\mbox{\scriptsize Complex}}$  3 reverts to dimer 1 in aqueous solutions (see the main text).

Page 26

Page 27

Table 2

Ni-K-Edge X-ray absorption parameters for complexes 2 and 5 and (Et<sub>4</sub>N)[Ni(nmp)(SR)] complexes.<sup>37–38</sup> Shell is the chemical unit defined for the multiple scattering calculation.  $R_{as}$  is the metal-scatterer distance.  $\sigma_{as}^2$  is a mean square deviation in  $R_{as}$ .

Gale et al.

Complex	¤	shell	$\overset{\boldsymbol{R}}{(\mathring{A})}$	$\begin{matrix} \sigma_{as}^{2} \\ (\mathring{A}^2) \end{matrix}$	$\mathbf{f}_{\cdot a}$	$E_{0}\left(\mathrm{eV} ight)$	pre-edge peak (eV)	intensity
$K[Ni(GC-OMe)(S-p-C_6H_4CI)]$ (2)	-	Z-iZ	1.83	0.0024	0.088	8340	8335.8	0.31
	_	Z-ïZ	1.99	0.0024				
	2	Ni-S	2.16	0.0059				
K[Ni(GC-OMe)(SNAc)] (5)	-	N-iZ	1.83	0.0024	0.100	8340	8335.7	0.34
	-	Z-iZ	1.99	0.0024				
	2	Ni-S	2.17	0.0052				
$K[Ni(nmp)(S-p-C_6H_4C!)]$	-	Z-iZ	1.85	0.0024	0.075	8340	8337.6	0.42
	-	Z-iZ	1.97	0.0024				
	2	Ni-S	2.16	0.0045				
K[Ni(nmp)(S-o-babt)]	-	N-iN	1.86	0.0024	0.061	8340	8336.5	0.42
	_	Z-ïZ	1.96	0.0024				
	7	Ni-S	2.17	0.0028				
K[Ni(nmp)(S'Bu)]	1	Z-iZ	1.85	0.0024	0.076	8340	8336.4	0.35
	-	N-iN	1.97	0.0024				
	2	S-iN	2.16	0.0051				

 $<sup>^{\</sup>it a}$ f' is a normalized error (chi-squared):

$$f' = \frac{\left\{ \sum_{i} \left[ k^3 \left( \chi_i^{obs} - \chi_i^{calc} \right) \right]^2 / N \right\}}{\left[ \left( k^3 \chi^{obs} \right)_{min} - \left( k^3 \chi^{obs} \right)_{min} \right]}$$